Appl Phys B (2011) 105:293–300
DOI 10.1007/s00340-011-4694-x

Applied Physics B
Lasers and Optics

Control of chirped pulse trains: a *speedway* for free-optimization experiments

N.X. Truong · J. Tiggesbäumker · K.-H. Meiwes-Broer

Received: 10 March 2011 / Revised version: 28 June 2011 / Published online: 31 August 2011

Abstract Complex phase-only shaping of intense ultrashort laser pulses is applied to generate highly flexible pulse structures with regular envelopes. By incorporating the linear chirp as additional free parameter into the technique of colored pulses, trains of chirped pulses are produced, capable of independent and simultaneous modulation of relative intensity ratio, optical delay, and individual chirp. Such pulses might find applications in multi-parameter scans or closed-loop feedback measurements. For the latter, we demonstrate that with use of these tailored pulse trains, adaptive feedback control experiments quickly converge. They provide near-optimal solutions, already revealing key features of the system under study. Moreover, seeding standard free-optimization routines with these temporary solutions largely accelerates the search for the closest-possible optimum.

1 Introduction

Advances in optics over the last two decades have allowed to generate, measure, and control intense ultrashort laser pulses [1, 2]. With the advent of the optical frequency comb technique [3] in combination with pulse shaping methods, it is possible to produce optical arbitrary waveforms from a train of ultrashort pulses [4]. As a particular application, tailored pulses can be utilized to gain a coherent control over quantum mechanical processes such as ultrafast chemical reactions [5], or intense laser-matter interactions [6]. When integrated in a closed-loop feedback control scheme, adapted ultrashort optical waveforms can effectively promote a desired reaction (see, e.g., [7]). However, as a drawback, often a quite complex optimal pulse structure emerges in the experiment possibly showing nonrelevant substructures which cover the essential signatures. Reducing the degrees-of-freedom in the pulse shaping might be advantageous in such situations. Due to the restriction in the parameter space, the search process accelerates and a reduction in the complexity of the optimal pulse structures is obtained in a fraction of time of a free-optimization experiment (FOE) [8, 9]. The information content of course is lowered and the extracted physics might be too crude to fully resolve or entirely identify the leading terms necessary to guide the system along the optimal reaction pathway. Hence, hybrid techniques are appealing since they can combine the advantages of initially low parameter search routines with the flexibility of FOE. In following this idea, we introduce the method of generating laser pulses with simple envelopes to extract key signatures but high variability to closely follow the optimal reaction path. These are chirped pulse trains (ChPT), well-suited in applications as fast and versatile initial preoptimizing routines providing effective seeds for subsequent FO steps.

Extensive efforts have been devoted to the phase-only generation of pulse trains [10–15], currently used in, e.g., pump-probe, fitness landscape, or closed-loop coherent quantum control [16, 17]. In particular, they might be ap-

N.X. Truong (✉)
FOM—Institute for Atomic and Molecular Physics (AMOLF),
P.O.Box 41883, 1009 DB Amsterdam, The Netherlands
e-mail: tnguyen@amolf.nl

N.X. Truong
e-mail: truong@mbi-berlin.de

J. Tiggesbäumker · K.-H. Meiwes-Broer
Institut für Physik, Universität Rostock, 18051 Rostock, Germany

J. Tiggesbäumker
e-mail: josef.tiggesbaeumker@uni-rostock.de

K.-H. Meiwes-Broer
e-mail: meiwes@uni-rostock.de

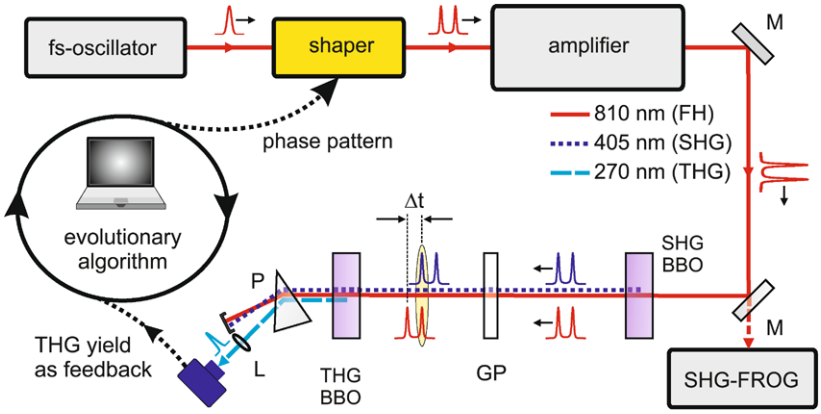

Fig. 1 Experimental setup for *double pulse-based* third-harmonic generation. The optimal laser pulse comprises two pulses of different intensity and chirp to achieve a high photon conversion efficiency. See the text and [9] for more details (*GP*, glass plate; *BBO*, nonlinear crystals)

plied to studies in which the temporal frequency distribution of the laser pulses is important, like intrapulse dumping [16, 18, 19], pump-dump scenarios [20], or intense laser-cluster interactions [17, 21–23]. We have recently described the method of generation of colored pulse trains (CPT) providing an independent and simultaneous modulation of relative intensity ratio and pulse separation [9]. It was shown that colored pulse trains are capable to quickly reveal the key characteristics of a system under investigation. However, the available parameter space of phase-only shaping was artificially truncated, i.e., *chirp modulation* was not considered. By extending the CPT method in this direction, a variable pulse forming scheme is introduced and one is equipped with a highly flexible but comprehensible handle, as we will demonstrate.

The paper proceeds as follows. In Sect. 2, the experimental setup to produce ChPT and the scheme for conducting the evolutionary search studies are presented. In Sect. 3, the mathematical description to generate chirped pulse trains is outlined and verified by comparison with experiments. Finally, we evaluate the ability of applying CPT and ChPT as seeds in adaptive feedback control studies.

2 Experimental details

The chirped pulse amplification (CPA) laser system consists of a sub-12 fs oscillator (MTS, KMLabs) and a multipass amplifier (Odin-II HE, Quantronix), delivering 35 fs pulses at a central wavelength of $\lambda_0 = 810$ nm ($\omega_0 = 2.33$ rad fs^{-1}) with energies of up to 2.5 mJ and a repetition rate of 1 kHz. Prior to amplification, a pulse shaper, an acousto-optic programmable dispersive filter-AOPDF (Dazzler, Fastlite), is employed to tailor both the spectral phase and amplitude of laser pulses. Details about the AOPDF technology can be found elsewhere [24]. Briefly, a controlled acoustic wave is launched along the ordinary axis of an acousto-optical crystal (TeO_2) forming a longitudinal transient grating [25]. By acousto-optic diffraction, different wavelengths of the optical pulse are switched onto the extraordinary axis at certain positions in the crystal. A phase modulation of the diffracted wave can thus be achieved by controlling the phase-matching conditions between acoustic and optical frequencies. With the 25 mm-long TeO_2 crystal, the AOPDF has a maximum adjustable group delay of 3 ps with a 0.6 nm spectral resolution and a number of adjustable parameters of up to ∼200. We note that by choosing the local sound level the intensity of the diffracted wave can be controlled. However, amplitude manipulation will not be considered in this work.

To fully characterize the tailored optical laser fields, a home-built SHG-FROG (second-harmonic generation frequency-resolved optical gating) apparatus is employed [26]. In addition to the time-domain representation, we choose a joint time-frequency distribution, i.e., the Husimi spectrogram [27], to give comprehensive views of the optical pulses.

A well-documented optical setup [16] for third-harmonic generation (THG) has been utilized as model system to illustrate the applicability of chirped multipulses in optimization experiments. We however slightly simplified the experimental arrangement as sketched in Fig. 1. In brief, the fundamental (FH, 810 nm) optical pulse from the CPA laser is frequency-doubled to 405 nm in a SHG crystal (100 µm-thick BBO). After leaving the crystal, the FH and SHG are temporally and spatially overlapped to generate the third-harmonic (270 nm) in a THG crystal (150 µm-thick BBO). The third-harmonic is then spatially separated from the other beams by a prism P (quartz) and detected by a high resolution spectrometer (HR4000, Ocean Optics). By inserting a piece of glass GP (SQ1) in between the nonlinear crystals, the FH shifts about $\Delta t \approx 310 \pm 20$ fs ahead of the SHG. This reduces their temporal overlap, leading to a significant decrease in the THG yield. We emphasize that although the optical setup is rather simple, it contains some special features attractive for the present studies: An efficient third-harmonic generation is obtained (i) only for double pulses with an appropriate optical delay, (ii) with more

intense leading pulses, and (iii) when the subpulse's chirp balances the phase-mismatches, e.g., developing in the nonlinear crystals.

To attain the optimal pulse structure giving the highest THG signal for the setup, a closed-loop feedback control scheme will be used, combining an evolutionary algorithm (EA) [21, 28] with the femtosecond pulse shaping techniques. In short, an initial population of N_p optical waveforms is created either at *random* or by *seeding*. Each waveform is encoded by a set of spectral phase parameters, and then evaluated through its THG yield (fitness value). Only the best waveforms with high fitness values have more chances to pass their "good" properties to the next generation. After each evolutionary step, a new population is produced via selection and subsequent modifications by applying recombination (crossover) and mutation operators. A run (cycle) is complete after a given number of generations or when the converging conditions, e.g., no further significant improvement of the best fitness, are fulfilled. The robustness and reliability of this type of EA have been proven in recent work [9, 21].

3 Mathematical description

In the frequency-domain, the original laser pulse can be defined by

$$\tilde{E}_{\mathrm{in}}(\omega) = |\tilde{E}_0(\omega)| \exp\bigl[-\mathrm{i}\psi(\omega)\bigr], \tag{1}$$

with a spectral amplitude $\tilde{E}_0(\omega)$ and an initial spectral phase $\psi(\omega)$ assumed to be zero, $\psi(\omega) \equiv 0$. A pulse shaper modifies the input pulse with spectral phase-only filters of the form $H(\omega) = \exp[-\mathrm{i}\Phi(\omega)]$, giving the output laser field

$$\tilde{E}_{\mathrm{out}}(\omega) = \tilde{E}_{\mathrm{in}}(\omega) \exp\bigl[-\mathrm{i}\Phi(\omega)\bigr]. \tag{2}$$

For simplicity, the spectral amplitude distribution is assumed to be Gaussian, i.e., $|\tilde{E}_0(\omega)| = E_0 \exp[-2\ln 2(\omega - \omega_0)^2/\Delta\omega^2]$, with $\Delta\omega$ the spectral full width at half maximum (for our laser system, $\Delta\omega \simeq 0.08$ rad fs^{-1}). The spectral phase $\Phi(\omega)$ is usually expanded into a Taylor series around ω_0 [29],

$$\Phi(\omega) = \varphi_0 + (\omega - \omega_0)\varphi_1 + (\omega - \omega_0)^2\varphi_2/2 + \cdots, \tag{3}$$

where φ_k $(k = 0, 1, 2, \ldots)$ denotes the expansion coefficient of the order k. The complex temporal electric field is then obtained by an inverse Fourier transformation, $E_{\mathrm{out}}(t) = \mathcal{F}^{-1}\{\tilde{E}_{\mathrm{out}}(\omega)\}$. According to the Fourier transform shift theorem [30], a linear term in the spectral phase, that is $\varphi_1 \equiv \tau$, leaves the laser field envelope unchanged, but shifts it in the time domain. Pulse trains can thus be formed by addressing different parts of the laser spectrum with certain values of τ [9]. We note that in general the shape of the single pulses is Gaussian but slightly modified by the *erf*-function [9, 15, 31]. Colored double pulses (C2P) for instance are produced by imposing a triangular spectral phase function [15, 31]:

$$\Phi_{\mathrm{C2P}}(\omega) = \frac{\tau}{2}|\omega - \omega_{\mathrm{br}}|, \tag{4}$$

where τ is the pulse separation and $\omega_{\mathrm{br}} = (\omega_0 + \delta\omega)$ is the spectral phase breakpoint, i.e., where the spectrum is split into a *red* $(\omega \in [-\infty, \omega_{\mathrm{br}}])$ and a *blue* $(\omega \in [\omega_{\mathrm{br}}, +\infty])$ part. A positive τ shifts the long wavelength region forward and the short wavelength region backward by $\tau/2$. This results in a colored double pulse with a leading red-shifted and a trailing blue-shifted subpulse, separated by an optical delay of τ. The breakpoint ω_{br} defines the spectral composition of each subpulse, and thus adjusts their relative intensity ratio. More general, a colored pulse train is generated by superimposing a certain number of triangular spectral phases with different values of τ and ω_{br} [9],

$$\Phi_{\mathrm{CPT}}(\omega) = \sum_{n=1}^{N} \Phi_{\mathrm{C2P}}^{(n)}(\omega) = \frac{1}{2}\sum_{n=1}^{N} \tau_n |\omega - (\omega_0 + \delta\omega_n)|. \tag{5}$$

While in CPT the pulse duration is nearly maintained [15, 31], the utilization of higher order terms $(k \geq 2)$ in the Taylor series (3) will give even more complex pulse structures and, e.g., will allow for a proper choice of the single pulse durations. This provides the essential flexibility to successfully implement the scheme into the following feedback control studies. Exemplarily, the method to generate chirped double pulses (Ch2P) having a simple linear chirp $(k = 2)$ at a spectral breakpoint ω_{br} is outlined. The corresponding spectral phase functions are addressed separately to the red and blue parts,

$$\begin{aligned}\Phi_{\mathrm{Ch2P}}(\omega) = {} & \frac{\tau}{2}|\omega - \omega_{\mathrm{br}}| \\ & + \varphi_2^{\mathrm{red}} \frac{1 - \mathrm{sign}(\omega - \omega_{\mathrm{br}})}{4}\bigl(\omega - \omega_0^{\mathrm{red}}\bigr)^2 \\ & + \varphi_2^{\mathrm{blue}} \frac{1 + \mathrm{sign}(\omega - \omega_{\mathrm{br}})}{4}\bigl(\omega - \omega_0^{\mathrm{blue}}\bigr)^2,\end{aligned} \tag{6}$$

with φ_2^{red} and $\varphi_2^{\mathrm{blue}}$ the linear chirp coefficients. In general, for the effective central (angular) frequencies $(\omega_0^{\mathrm{red}}, \omega_0^{\mathrm{blue}})$, the *intensity-weighted* averages [32] are used:

$$\begin{aligned}\omega_0^{\mathrm{red}} &= \frac{\int_{-\infty}^{\omega_{\mathrm{br}}} |\tilde{E}_0(\omega)|^2 \omega \,\mathrm{d}\omega}{\int_{-\infty}^{\omega_{\mathrm{br}}} |\tilde{E}_0(\omega)|^2 \,\mathrm{d}\omega}, \\ \omega_0^{\mathrm{blue}} &= \frac{\int_{\omega_{\mathrm{br}}}^{\infty} |\tilde{E}_0(\omega)|^2 \omega \,\mathrm{d}\omega}{\int_{\omega_{\mathrm{br}}}^{\infty} |\tilde{E}_0(\omega)|^2 \,\mathrm{d}\omega}.\end{aligned} \tag{7}$$

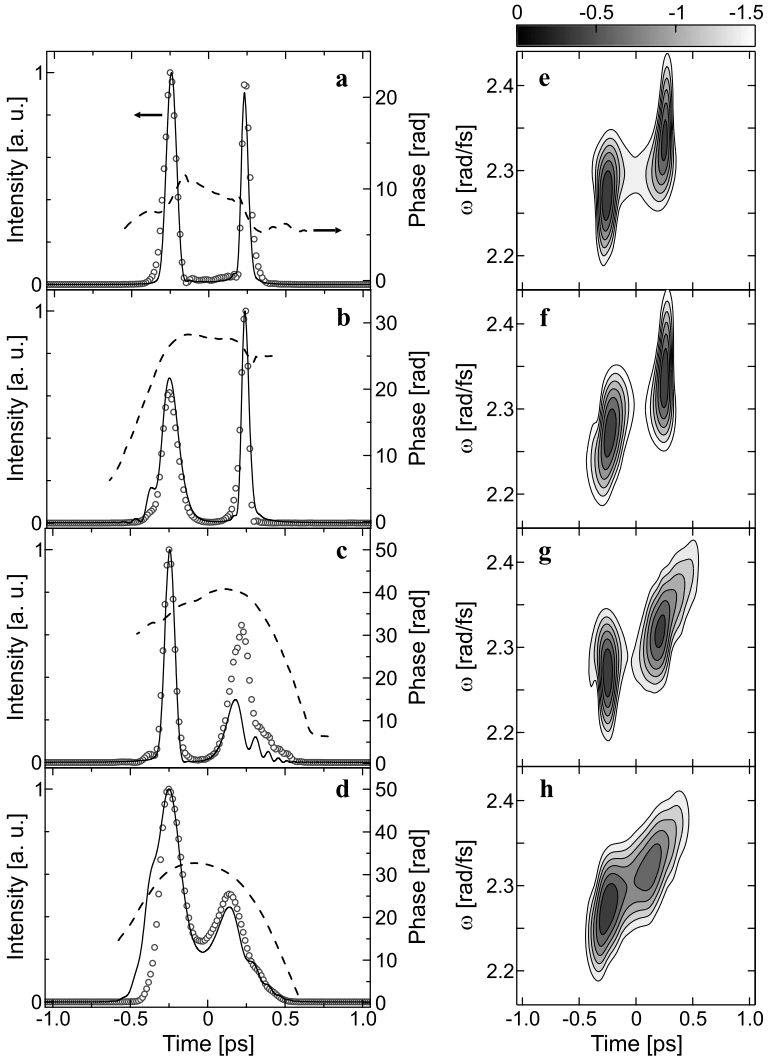

Fig. 2 FROG measurements of chirped double pulses tailored with linear chirp coefficients (φ_2^{red}, φ_2^{blue}): (**a**) (0 fs^2, 0 fs^2), (**b**) (4000 fs^2, 0 fs^2), (**c**) (0 fs^2, 4000 fs^2), and (**d**) (5000 fs^2, 5000 fs^2). The pulse separation and spectral phase breakpoint are fixed to $\tau = 500$ fs and $\omega_{\text{br}} = \omega_0$, respectively. *Left column*: experimental intensity (*circles*) and phase (*dashed lines*) vs. time. The calculated intensity profiles (*solid lines*) based on the computed spectral phases are included for comparison. Notably, nonlinear distortions in the CPA system lead to slight differences in amplitude between experiment and simulation. Small wings in the subpulses are due to the abruptly truncated shapes of the spectral regions. *Right column*: the corresponding Husimi distributions, which intuitively display the chirp characteristics of the shaped pulses

However, for $\omega_{\text{br}} = \omega_0$, we can simply identify ω_0^{red} (ω_0^{blue}) with the momentary frequency at $-\Delta\tau/2$ ($\Delta\tau/2$) as introduced for colored double pulses in [31], i.e., $\omega_0^{\text{red}} = \omega_0 - \Delta\omega/\sqrt{2\pi \ln 2}$, and $\omega_0^{\text{blue}} = \omega_0 + \Delta\omega/\sqrt{2\pi \ln 2}$.

To illustrate the capabilities of chirped pulses, Fig. 2 shows examples of double pulses separated by $\tau = 500$ fs for different chirp values (φ_2^{red}, φ_2^{blue}). Corresponding numerical estimations are also provided for comparison, which are based on the computed spectral phase function $\Phi_{\text{Ch2P}}(\omega)$ and a measured amplified spectrum (instead of a Gaussian-assumed one). For further simplicity, nonlinear distortions through propagation in the amplifier are neglected in the calculations. These might account for slight differences in the experimental and simulated temporal intensity profiles. Nonlinear effects in the CPA such as gain narrowing or self-phase modulation might lead to the redistribution of the laser energy in the amplified double pulse and hence the change of the relative intensity ratios (see [9] for further discussion).

The good agreement in between experiment and simulation makes us confident that one can also assign the experimental values of φ_2^{red} and φ_2^{blue} directly to the programmed ones. This is demonstrated in Fig. 3. Variations mainly result from the shape of the *erf*-function which introduces small distortions on the pulse (see [9, 15, 31] for mathematical details). In addition, a nonzero initial phase (1) might contribute. It is straightforward to extend the method to pulse trains. Superimposing a number of spectral phase functions $\Phi_{\text{Ch2P}}(\omega)$ enables to systematically generate complex structured pulses which, however, consist of simple pulse envelopes unless higher chirp coefficients ($k > 2$) are considered.

4 Results and discussion

The flexibility of CPT and Ch2P in generating simple pulse sequences—which however might be highly complex struc-

Table 1 Different encoding methods for spectral phase functions in systematic and adaptive feedback control experiments. CDPFL: systematic pulse modulation of optical delay and intensity ratio giving the colored double pulse fitness landscape; CPT: five-pulse sequences with a simultaneous modulation of relative intensity ratios and pulse separations; Ch2P: chirped double pulses with simultaneous manipulation of the relative intensity ratio, pulse delay, and linear chirps of the subpulses; FO: unrestricted pulse shaping (free-optimization) with use of 128 parameters, regularly distributed across the spectrum to form the spectral phase function

Method	Phase function	Parameters	Parameter ranges
CDPFL	$\Phi_{\mathrm{C2P}}(\omega)$, (4)	$\{\tau, \delta\omega\}$	$\{[-1.5\ \mathrm{ps}, 1.5\ \mathrm{ps}],$ $[-150\ \mathrm{rad\,ps^{-1}}, 150\ \mathrm{rad\,ps^{-1}}]\}$
CPT	$\Phi_{\mathrm{CPT}}(\omega)$, (5)	$\{\tau_n, \delta\omega_n\},$ $n = [1, 4]$	$\{[-1\ \mathrm{ps}, 1\ \mathrm{ps}],$ $[-150\ \mathrm{rad\,ps^{-1}}, 150\ \mathrm{rad\,ps^{-1}}]\}_n$
Ch2P	$\Phi_{\mathrm{Ch2P}}(\omega)$, (6)	$\{\tau, \delta\omega, \varphi_2^{\mathrm{red}}, \varphi_2^{\mathrm{blue}}\}$	$\{[-1\ \mathrm{ps}, 1\ \mathrm{ps}],$ $[-150\ \mathrm{rad\,ps^{-1}}, 150\ \mathrm{rad\,ps^{-1}}],$ $[-10^4\ \mathrm{fs^2}, 10^4\ \mathrm{fs^2}], [-10^4\ \mathrm{fs^2}, 10^4\ \mathrm{fs^2}]\}$
FO	$\Phi_{\mathrm{FO}}(\omega_n) = \Phi_n$	$\{\Phi_n\}, n = [1, 128]$	$\{[0, 2\pi]\}_n$

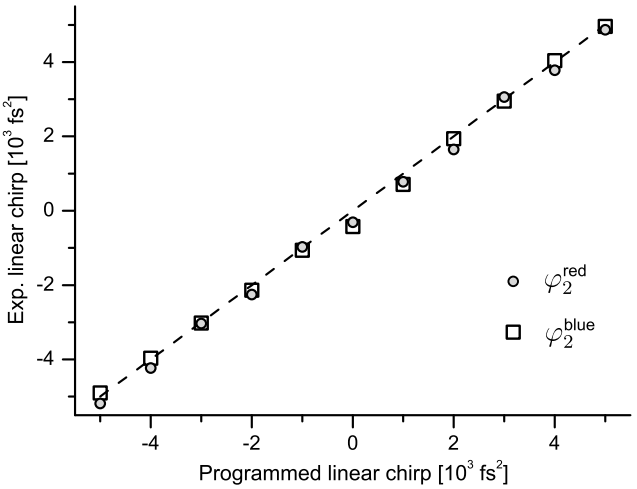

Fig. 3 Dependence of the experimental linear chirp ($\varphi_2^{\mathrm{red}}, \varphi_2^{\mathrm{blue}}$) on the initial values transferred to the pulse shaper for the generation of chirped double pulses. The proximity of both φ_2 to the bisecting line suggests that the experimental φ_2 is directly related to the spectral chirp coefficient imprinted on the pulse by the shaper

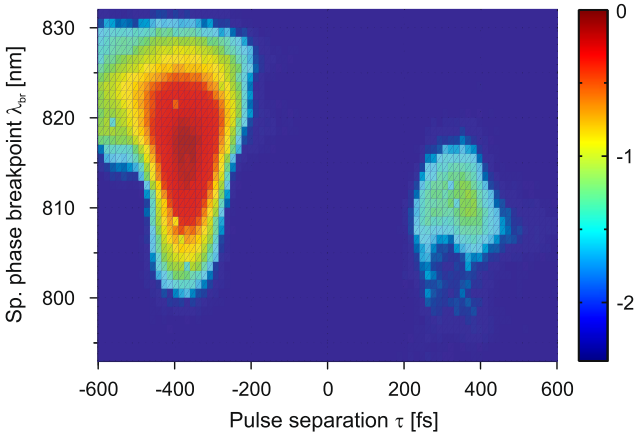

Fig. 4 THG fitness landscape measurement (CDPFL) obtained by tailoring through triangular spectral phase functions with pulse separation τ and spectral phase breakpoint λ_{br} (see Fig. 1). The yield Y_{CDPFL} at the optimal setting ($\tau \simeq -365$ fs, $\lambda_{\mathrm{br}} \simeq 817$ nm) is taken as a reference measure for success of the optimizations presented below

tured internally—will help to resolve a number of optimization problems. The key idea is to start with an educated guess which roughly reflects the expected number of reaction steps to specify the number of subpulses. Based on these, restricted optimizations are performed to quickly discard low-fitness solutions. The subsequent free-optimization routine is then well equipped with a basic knowledge about the system under study. By fine-tuning the available parameters, the pulse structure giving the highest fitness might be obtained. We will see that, in conducting such an experimental scheme, the total number of generations necessary for the algorithm to converge can largely be reduced. As a proof of principle experiment we use the setup described in Sect. 2 and validate the different basic approaches.

Following the work of Vogt et al. [16], we first applied the colored double pulse fitness landscape method (CDPFL) to find the pulse configurations leading to a maximum THG yield. These solutions will serve as references for the closed-loop measurements shown below. In CDPFL, a fitness value is *systematically* recorded as function of pulse separation τ and spectral phase breakpoint $\lambda_{\mathrm{br}} = 2\pi c/\omega_{\mathrm{br}}$ (see Table 1 and (4)). The technique is similar to pump-probe delay scans, but provided with additional possibilities of, e.g., adjusting the relative intensity ratio. Figure 4 shows the result of the CDPFL measurement on the model system with the THG yield taken as fitness. The landscape has a pronounced maximum found at $\tau \simeq -365$ fs and $\lambda_{\mathrm{br}} \simeq 817$ nm. The corresponding laser pulse analyzed with FROG is illustrated in

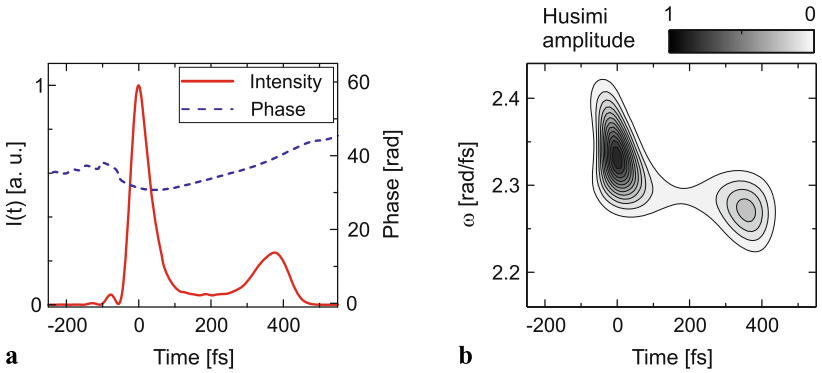

Fig. 5 Optimal pulse shape with an asymmetric double pulse structure leading to the maximum THG yield in the CDP fitness landscape (Fig. 4): (**a**) measured intensity and phase vs. time, (**b**) the corresponding Husimi representation showing a clear red-shift of the trailing pulse

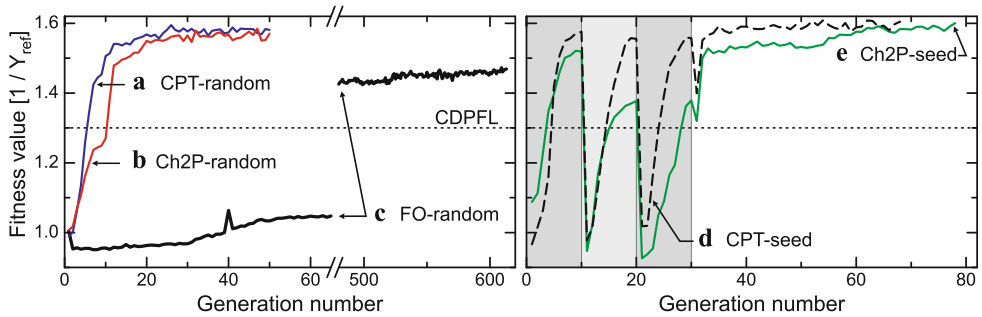

Fig. 6 Evolution of the averaged best fitness for different THG-maximizing procedures. Left: random starts using (*a*) CPT-, (*b*) Ch2P-, and (*c*) FO-encoding. *Right*: (*d*) CPT- and (*e*) Ch2P-seeded free-optimization. The data points represent the mean fitness values of the ten best individuals extracted after each generation. For comparison, the optimal yield found by CDPFL, Y_{CDPFL}, is depicted (*dotted lines*). The *shaded areas* (ten generations each) indicate different runs with a random start of a restricted optimization to find seeds for the subsequent free-optimization

Table 2 Extracted parameters of the optimal double pulses corresponding to the CDPFL and optimization measurements shown in Fig. 5 and Fig. 6, respectively. τ_{p1} and τ_{p2}, temporal widths of the leading and trailing pulses; Δt, double-pulse delay; I_2/I_1, relative intensity ratio between trailing and leading pulse. The respective optimal THG yields are compared to the maximum signal provided by the fitness landscape experiment through an optimization factor, $\mathcal{K} = Y_{\mathrm{opt}}/Y_{\mathrm{CDPFL}}$. All relative errors are <3%

Method	τ_{p1} (fs)	τ_{p2} (fs)	Δt (fs)	I_2/I_1	$\mathcal{K}$
CDPFL	64	120	365	0.24	1.00
CPT, random	51	101	349	0.33	1.14
Ch2P, random	53	96	331	0.37	1.14
FO, random	38	93	355	0.27	1.13
FO, CPT-seed	51	104	358	0.30	1.22
FO, Ch2P-seed	52	93	347	0.35	1.25

Fig. 5, showing an asymmetric double pulse structure with a clearly red-shifted trailing pulse (see also Table 2).

Whereas in CDPFL only two parameters are varied, the full parameter hyperspace can be explored when a free-optimization experiment is conducted. Applying the closed-loop feedback control scheme [33] by adaptively modifying the spectral phase $\Phi(\omega)$ (see Table 1), the impacts of a multitude of different laser fields are probed, finally giving an adapted laser field representing the optimal solution. Several strategies have been evaluated, which differ by their possible pulse shapes or by how the initial population is created. To start the FO, for instance, an initial population of $N_{\mathrm{p}} = 50$ waveforms is created at random through an appropriate encoding. A THG-reference signal Y_{ref} produced with a 300 fs double pulse was recorded in each generation to monitor the experimental conditions. Figure 6c shows the result of the free-optimization experiment performed on the model system. Obviously, the full optimization improves the THG yield compared to the systematic but few-parameter CDPFL scan. However, the convergence of the full optimization is rather slow, approaching a fitness value of 1.5 only after about 600 generations.

As briefly mentioned in Sect. 1, restricted and free optimization have complementary features. One can profit from the simplicity but variability of pulse trains and incorporate these properties into FO. For this reason, we split the EA routine and start with an initial signal maximization by applying colored pulse sequences to quickly find temporal solutions with high fitness. Thereafter, the full-parameter optimizations are seeded with these adaptively found CPTs or Ch2Ps. A train of five subpulses is chosen for CPT, whereas for chirped pulses only double pulses are considered. Details about the corresponding parameter ranges are summarized

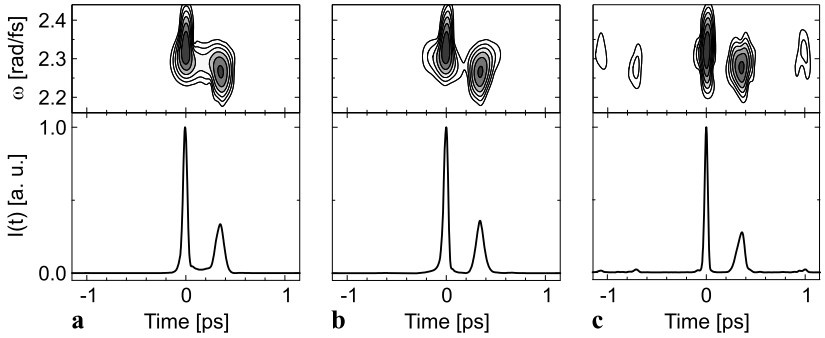

Fig. 7 Optimal pulses obtained by adaptively maximizing the THG yield using different optimization methods presented in Fig. 6: (*left*) random start with use of colored five-pulse trains (cf. Fig. 6a), (*middle*) seeded start employing chirped double pulses (cf. Fig. 6e), (*right*) 128-parameter FO (cf. Fig. 6c). *Top*: Husimi distributions (logarithmic scale), *bottom*: the corresponding temporal intensities $I(t)$

in Table 1. Note that the latter seed is directly adapted to the expected number of subpulses relevant to obtain the optimal solution, while in CPT the number of subpulses is largely overdetermined.

The hybrid EA initially starts in a random mode ($N_p = 30$) using either CPT- or Ch2P-encoding for a number of cycles ($N_{run} = 3$, ten generations each). The five best waveforms (seeds) obtained from this procedure will be chosen and then mixed into a pool of other 45 randomly created individuals to form an initial population ($N_p = 50$) for a subsequent unrestricted (free) closed-loop feedback control (128-parameter FO). Note that once running into a local optimum, the EA might sooner escape this when working in a restricted optimization mode, rather than in the unrestricted one. It is therefore beneficial to operate the initial EA code with a small population of different laser pulses and more cycles before switching to the free-optimization scheme.

Five different adaptive feedback experiments have been performed to maximize the THG yield, including: random starts using (a) CPT-, (b) Ch2P-, and (c) FO-encoding, and seeded starts with (d) CPT-, and (e) Ch2P-encoding. The progress of all optimal searches is displayed in Fig. 6. The results show that, irrespective of CPT- or Ch2P-encoding, the seeded method indeed improves the best yields when compared to routines using a random start only. When appropriately seeded, the free-optimization search maximizes the yield within only about 20 generations, instead of over 600 as in pure FO. In addition, essentials of the expected final laser pulse configuration crystallize out of the seeded FO pulse structure search. Similar to the CDPFL result (Fig. 5), the adaptively determined pulses also show a dominant asymmetric double pulse structure as exemplarily displayed in Fig. 7. In the pure FO (Fig. 7c) instead, additional substructures are present indicating that the optimization is incomplete. However, the dominant subpulses are present with slightly reduced temporal widths when compared to the CPT and Ch2P-seed optimizations. It is interesting to note that seeded and pure FO reveal different aspects, each of them guiding towards the optimal solution, thus possibly leading to enrichments in the understanding of the reaction in detail. The analysis of the optimal pulses provided by the chosen methods is summarized in Table 2.

In principle the hybrid algorithm can be applied to any process, providing that an appropriate spectral phase function can be constructed for seeding. For instance, an extreme complex spectral phase produced through filamentation [3] can roughly be compensated with use of a Taylor series of up to a suitable kth order (3). Although solutions found by systematic parameter-scans might be taken as seeds for hybrid optimizations, we suggest to use random start procedures with a proper encoding (or any stochastic search method capable to find the global optimum, e.g., simulated annealing [34]) to avoid local maxima.

5 Conclusions

By phase-only shaping different parts of the spectrum of ultrashort laser pulses with individual spectral phase functions of high orders, chirped pulse trains can be generated. On the one hand, these provide a high variability and control in the choice of pulse separations, intensity ratios, and linear chirps of the subpulses. The flexibility in tailoring such laser pulses opens up the possibility to find near-optimal solutions using open-loop or restricted closed-loop optimization measurements with adapted number of parameters and well-defined initial structure. In the present work, the method has been demonstrated on a purely optical issue. We, however, expect that a number of spectroscopic applications, e.g., in femtosecond pump-probe (or -dump) experiments [16, 35–39] or laser-cluster interactions [17, 21], might benefit from the ChPT-approach. Chirp effects on the response of molecular systems to intense laser fields have been observed for pump [40–43] or probe (dump) [20, 38] pulses. It is therefore definitely interesting to perform systematic scans of different parameterizations in order to get additional insight into the molecular dynamics.

On the other hand, by seeding unrestricted optimizations with chosen pulse configurations, the search speed of the hybrid algorithm is remarkably improved, making it an appealing method for the optimization of experimental conditions with considerable target fluctuations like the intense laser interaction with metal clusters [44]. As an advantage of the preselection, most likely unphysical contributions, normally leading to gratuitous signatures in the optimal pulses, are significantly suppressed. Hence, the speed-up in the optimization search and the possible early disentangling of the basic mechanisms suggest that the proposed scheme will support future work, e.g., guiding to solutions of current problems in coherent quantum control (see [45] for a recent overview).

Acknowledgements We thank Gustav Gerber for stimulating discussions and his continuous support to our work. Funding by the Deutsche Forschungsgemeinschaft through the Sonderforschungsbereich 652 is gratefully acknowledged.

References

1. U. Keller, Nature **424**, 831 (2003)
2. F. Krausz, M. Ivanov, Rev. Mod. Phys. **81**, 163 (2009)
3. J. Ye, S.T. Cundiff (eds.), *Femtosecond Optical Frequency Comb: Principle, Operation, and Applications* (Springer Science, New York, 2005)
4. S.T. Cundiff, A.M. Weiner, Nat. Photonics **4**, 760 (2010)
5. P. Nuernberger, G. Vogt, T. Brixner, G. Gerber, Phys. Chem. Chem. Phys. **9**, 2470 (2007)
6. T. Fennel, K.-H. Meiwes-Broer, J. Tiggesbäumker, P.-G. Reinhard, P.M. Dinh, E. Suraud, Rev. Mod. Phys. **82**, 1793 (2010)
7. R. Levis, G. Menkir, H. Rabitz, Science **292**, 709 (2001)
8. A. Bartelt, T. Feurer, L. Wöste, Chem. Phys. **318**, 207 (2005)
9. N.X. Truong, J. Tiggesbäumker, K.H. Meiwes-Broer, J. Opt. **12**, 115201 (2010)
10. A.M. Weiner, Rev. Sci. Instrum. **71**, 1929 (2000)
11. A. Weiner, S. Oudin, D. Leaird, D. Reitze, J. Opt. Soc. Am. A **10**, 1112 (1993)
12. A. Weiner, D. Leaird, Opt. Lett. **15**, 51 (1990)
13. P. Nuernberger, G. Vogt, R. Selle, S. Fechner, T. Brixner, G. Gerber, Appl. Phys. B **88**, 519 (2007)
14. D. Pestov, V.V. Lozovoy, M. Dantus, Opt. Express **17**, 14351 (2009)
15. M. Renard, R. Chaux, B. Lavorel, O. Faucher, Opt. Express **12**, 473 (2004)
16. G. Vogt, P. Nürnberger, R. Selle, F. Dimler, T. Brixner, G. Gerber, Phys. Rev. A **74**, 033413 (2006)
17. N.X. Truong, S. Göde, J. Tiggesbäumker, K.-H. Meiwes-Broer, Eur. Phys. J. D **63**, 275 (2011)
18. S. Ashworth, T. Hasche, M. Woerner, E. Riedle, T. Elsaesser, J. Chem. Phys. **104**, 5761 (1996)
19. G. Cerullo, C. Bardeen, Q. Wang, C. Shank, Chem. Phys. Lett. **262**, 362 (1996)
20. G. Vogt, P. Nuernberger, T. Brixner, G. Gerber, Chem. Phys. Lett. **433**, 211 (2006)
21. N.X. Truong, P. Hilse, S. Göde, A. Przystawik, T. Döppner, T. Fennel, T. Bornath, J. Tiggesbäumker, M. Schlanges, G. Gerber, K.H. Meiwes-Broer, Phys. Rev. A **81**, 013201 (2010)
22. A. Moore, K. Mendham, D. Symes, J. Robinson, E. Springate, M. Mason, R. Smith, J. Tisch, J. Marangos, Appl. Phys. B, Lasers Opt. **80**, 101 (2005)
23. Y. Fukuda, K. Yamakawa, Y. Akahane, M. Aoyama, N. Inoue, H. Ueda, Y. Kishimoto, Phys. Rev. A **67**, 061201 (2003)
24. F. Verluise, V. Laude, Z. Cheng, C. Spielmann, P. Tournois, Opt. Lett. **25**, 575 (2000)
25. A. Yariv, P. Yeh, *Optical Waves in Crystals* (Wiley, New York, 1984)
26. N.X. Truong, J. Tiggesbäumker, T. Döppner, Meas. Sci. Technol. **21**, 085303 (2010)
27. F. Grossmann, *Theoretical Femtosecond Physics—Atoms and Molecules in Strong Laser Fields* (Springer, Berlin, 2008)
28. H. Pohlheim, *Evolutionäre Algorithmen: Verfahren, Operatoren und Hinweise für die Praxis* (Springer, Berlin, 2000)
29. R. Trebino, *Frequency-Resolved Optical Gating: The Measurement of Ultrashort Laser Pulses* (Kluwer Academic, London, 2000)
30. R.N. Bracewell, *The Fourier Transform and Its Applications* (McGraw-Hill, New York, 2000)
31. P. Nuernberger, Opt. Commun. **282**, 227 (2009)
32. J.-C. Diels, W. Rudolph, *Ultrashort Laser Pulse Phenomena* (Academic Press, London, 2006)
33. R. Judson, H. Rabitz, Phys. Rev. Lett. **68**, 1500 (1992)
34. S. Kirkpatrick, C. Gelatt, M. Vecchi, Science **220**, 671 (1983)
35. T.C. Gunaratne, X. Zhu, V.V. Lozovoy, M. Dantus, Chem. Phys. **338**, 259 (2007)
36. S. Rausch, T. Binhammer, A. Harth, F.X. Kaertner, U. Morgner, Opt. Express **16**, 17410 (2008)
37. S. Bonora, D. Brida, P. Villoresi, G. Cerullo, Opt. Express **18**, 23147 (2010)
38. P. Marquetand, P. Nuernberger, G. Vogt, T. Brixner, V. Engel, Europhys. Lett. **80**, 53001 (2007)
39. M. Wollenhaupt, M. Krug, J. Koehler, T. Bayer, C. Sarpe-Tudoran, T. Baumert, Appl. Phys. B **95**, 245 (2009)
40. C.J. Bardeen, Q. Wang, C.V. Shank, Phys. Rev. Lett. **75**, 3410 (1995)
41. C.J. Bardeen, Q. Wang, C.V. Shank, J. Phys. Chem. A **102**, 2759 (1998)
42. G. Lanzani, M. Zavelani-Rossi, G. Cerullo, D. Comoretto, G. Dellepiane, Phys. Rev. B **69**, 134302 (2004)
43. A. Wand, S. Kallush, O. Shoshanim, O. Bismuth, R. Kosloff, S. Ruhman, Phys. Chem. Chem. Phys. **12**, 2149 (2010)
44. T. Fennel, T. Döppner, J. Passig, C. Schaal, J. Tiggesbäumker, K.-H. Meiwes-Broer, Phys. Rev. Lett. **98**, 143401 (2007)
45. C. Brif, R. Chakrabarti, H. Rabitz, New J. Phys. **12**, 075008 (2010)